

A new 1–2 GeV/c separated beam for BNL *

P.H. Pile, D. Beavis, R.L. Brown, R. Chrien, G. Danby, J. Jackson, D.M. Lazarus,
W. Leonhardt, C. Pearson, A. Pendzick, P. Montemurro, T. Russo, J. Sandberg, R. Sawafta,
C. Spataro and J. Walker

Brookhaven National Laboratory Associated Universities, Inc., Upton, NY 11973, USA

H.A. Enge

Massachusetts Institute of Technology, Cambridge, MA 02139, USA

Received 30 March 1992

A 1–2 GeV/c beam line has been constructed at the Brookhaven National Laboratory alternating gradient synchrotron (BNL AGS). The beam line is optimized to deliver an intense clean beam of 1.8 GeV/c negative kaons for an H particle search experiment and incorporates two stages of velocity selection with the magnetic optics corrected to third order. Details of the beam line design as well as results of the commissioning will be discussed.

1. Introduction

Experiments requiring intense beams of kaons have generally been limited by the presence of unwanted particles accompanying the beam. These unwanted particles (pions, muons, electrons and protons) are a result of direct production, slit scattering, and hyperon or meson decays. Beam lines with momenta up to a few GeV/c generally incorporate an $E \times B$ velocity filter (Wien filter) to help reduce the number of unwanted particles but invariably transmit more unwanted particles than kaons. For example, at 800 MeV/c the LESB I beam line at the BNL AGS typically has a $(\pi^- \mu^- e^-)/K^-$ ratio of 10:1 [1] and at lower momenta the ratio becomes worse. Most unwanted particles are pions and muons. Other examples include the K2 [2] and K3 [3] beam lines at KEK. Both K2 and K3 are single separation stage kaon beam lines. K2 operates in the 1–2 GeV/c momentum range while K3 operates up to 0.8 GeV for kaons. K2 is reported to run with a $(\pi^- \mu^- e^-)/K^-$ ratio of 5:1 at 1.6 GeV/c, while K3 operates with a $(\pi^- \mu^- e^-)/K^-$ ratio of about 10:1 at 0.6 GeV/c.

We have constructed a beam line at the BNL AGS that can deliver clean, intense beams of kaons in the 1–2 GeV/c range. The beam line incorporates two stages of separation, state of the art separators, optics

corrected to third order, and specialized collimators. In contrast to past beam lines, the beam purity increases dramatically as the beam momentum is lowered. In fact at 1.0 GeV/c the $(\pi^- \mu^- e^-)$ to kaon ratio is better than 1:10. The only other two-stage separated beam operating at this time is the K4 beam line [4] at KEK. The K4 beam line incorporates the K3 beam line as a first separation stage and includes a second stage of separation along with a second mass slit. This antiproton beam line is too long (28.5 m) to efficiently transport kaons since its kaon decay factor is greater than 100 at 0.8 GeV/c, its maximum momentum. The K4 beam line does, however, demonstrate the effectiveness of a second stage of separation. The measured [4] $(\pi^- \mu^- e^-)/\bar{p}$ ratio of 7–8:1 between 500 and 600 MeV/c is about a factor of 20–40 better than using K3 alone.

2. Beam line design

2.1. Design goals

The beam line design was optimized for use in experiments that study doubly strange ($S = -2$) systems. Detailed studies of such systems require an intense beam of negative kaons that is relatively free of other particles. Furthermore, in most cases, the K^- must be identified and its momentum determined on an event-by-event basis. Thus, various detectors must be accommodated into the beam line design.

* Work performed under the auspices of the US Department of Energy.

The beam momentum range was chosen to include the production cross section maximum for the $p(K^-, K^+) \Xi^-$ reaction, a reaction that transfers two units of strangeness to the proton. The peak in the cross section occurs at about a 1.8 GeV/c K^- momentum [5].

The following design goals were established:

- 1) The beam line should be capable of delivering 1×10^6 , 1.8 GeV/c K^- particles/AGS beam spill.
- 2) The beam purity should approach 1:1 unwanted particles to kaons.
- 3) The beam design should allow beam detectors (timing scintillators, hodoscopes, drift chambers, etc.) to be inserted without causing a significant deterioration in either beam intensity or purity.

In order to meet the first goal, the AGS proton beam intensity and beam line acceptance had to be considered together. Typically the AGS delivers $1.5-2.0 \times 10^{13}$ protons in a 1.2 s spill every 2.5 s. The beam is normally divided among four primary beam lines. In the near future, the intensity is expected to increase to about 6×10^{13} protons/spill after the booster [6] is fully commissioned (1992) and the AGS rf upgrade [7] is complete (~ 1995). If one assumes the new beam line will receive $0.5-1.0 \times 10^{13}$ protons/spill then, using Sanford-Wang [8] kaon production estimates, the beam line solid angle-momentum acceptance must be about 2-4 msr % to deliver 10^6 , 1.8 GeV/c K^- /spill (30 m beam length assumed). The decay factor for 1.8 GeV/c kaons is 7.1%/m, so beam length is a consideration.

Since conventional beam line designs have not been able to deliver beams with the desired purity, improvements were required. Conventional beam lines with only one separation stage cannot eliminate background

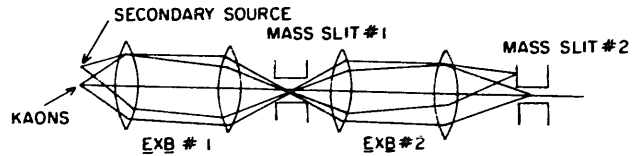


Fig. 1. The effect of two stages of velocity selection on secondary sources.

sources that originate away from the kaon production target. The velocity filter will sweep some of these secondary sources through the mass slit opening to the experimenter's target. The addition of a second stage of separation will help to eliminate such sources. The effect of two stage separation is illustrated in fig. 1. This approach has the added advantage that most unwanted particles will stop in the first mass slit, well away from the experimenter's target area.

The particle separation quality at the mass slits is dependent on the separator electric field strength (and plate length) and the vertical image size at the mass slits. In order to maximize the electric field, KEK style separators [2,9], with power supplies closely coupled to the separator tanks, were chosen (see section 2.5). Furthermore, in order to minimize the vertical beam width at the mass slits, the beam optics were partially corrected to third order.

In order to meet the third design criterion, the detectors need to be located near a horizontal and vertical focus to minimize the effect of multiple scattering. Furthermore, with 10^{13} protons/spill in the production target, the pion rate will approach 10^9 /spill. The detectors then must be located downstream of the first mass slit to minimize high rate problems.

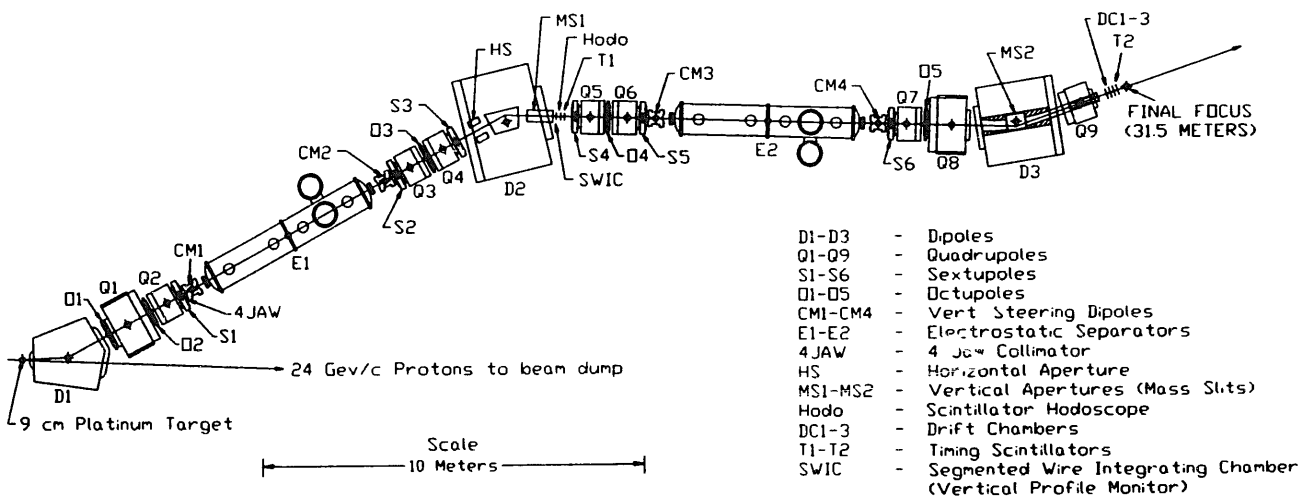


Fig. 2. A plan view of the 2 GeV/c beam line as configured for the commissioning run. The beam line concrete and steel shielding are not shown, as well as a low energy muon beam channel which views the same production target. Not shown in the figure is a drift chamber located between T1 and S4.

Table 1

Elements of the beam line. BNL designation for dipoles, 30D72 stands for 30 in. pole width by 72 in. long; quadrupoles, sextupoles and octupoles 12Q30 means 12 in. diameter by 30 in. long pole tip. Positive and negative quadrupole pole tip fields refer to horizontal and vertical focusing elements respectively

Dipole	BNL Designation	Gap [cm]	Effective length [m]	Field [kG] at 1.0 GeV/c	Bend [deg]
D1	Sector	7.62	1.91 ^a	13.95	25.5
D2	30D72	15.24	2.00	–15.69	–30.0
D3	18D72	15.24	1.99	10.0	19.0
Quadrupoles	BNL Designation		Assumed effective length [cm]		Pole tip field [kG]
Q1	12Q30		88.01		8.67
Q2	12Q16		50.11		–11.87
Q3	12Q16		50.11		–3.13
Q4	12Q16		50.11		1.21
Q5	12Q16		50.11		7.38
Q6	12Q16		50.11		–9.04
Q7	12Q16		50.11 ^a		–11.23
Q8	12Q30		89.15 ^a		7.41
Q9	8Q24		69.8		–11.57
Sextupoles	BNL Designation		Assumed effective length [cm]		Pole tip field [kG]
S1	12S5		21.6		–0.205
S2	12S5		21.6		+2.56
S3	12S5		21.6		–1.36
S4	12S5		21.6		–0.50
S5	12S5		21.6		+1.38
S6	12S5		21.6		–0.15
Octupoles	BNL Designation		Assumed effective length [cm]		Pole tip field [kG]
01	1202		12.7		–1.5
02	1202		12.7		0.9
03	1202		12.7		0.5
04	1202		12.7		0.5
05	1202		12.7		0.25
Separators	Width [cm]	Gap [cm]	Assumed effective length [m]		Voltage [kV]
E1	40	10	4.6		750
E2	40	10	4.6		–750
Correction dipoles	BNL designation	Gap [cm]	Assumed effective length [cm]		Field [kG]
CM1–4	8D8	20.3	36.3 ^a		1.59
Moveable collimators	Purpose		Material		Length [cm]
Four-jaw	θ – ϕ collimator		Copper		35
HS	momentum collimator		Hevimet		40
MS1	vertical mass slit		Hevimet		90
MS2	vertical mass slit		Hevimet		90
Target	Length [cm]	Width [cm]	Height [cm]		Cooling
Platinum	9	0.7	1.0		Water cooled copper base

^a Actual measured effective length.

2.2. General features

A schematic of the beam line is shown in fig. 2 and a list of beam line elements is given in table 1. The elements in table 1 are grouped by generic type. Second and third order correction elements were inserted as discrete components designed and built for this beam line. The D1 sector magnet is also a special magnet unique to this line. All other magnets are standard BNL quadrupoles and dipoles [10].

AGS protons (nominally 24–30 GeV/c) are incident on a 9 cm thick platinum production target located at the entrance to the first dipole. The 0.7 cm horizontal by 1.0 cm vertical cross section target is silver soldered to a copper support block that rests on a water cooled base. The target can withstand $\leq 1.5 \times 10^{13}$ 24 GeV/c protons per 1.2 s AGS spill every 2.5 s. The dipole (D1 in fig. 2) serves to bend the secondary beam away from the proton beam, which is currently dumped into iron and concrete shielding after it exits D1. D1 incorporates mineral insulated coils, built in-house, capable of withstanding the high radiation levels that will result from the 10^{13} proton/spill target station.

The secondary beam is transported in vacuum to the first mass slit (MS1) entrance and then through a 0.0076 cm thick aluminum window into air to the entrance of sextupole S4. The space between MS1 and S4 is reserved for experimental detectors, consisting of a vertical profile monitor, a 0.64 cm thick timing scintillator, a 0.64 cm thick scintillator hodoscope and a drift chamber for the commissioning run. The beam is then transported in vacuum through the second mass slit (MS2) to the exit of the last quadrupole, Q9. The primary purpose of the second dipole is to bend the beam and thus allow the beam line to be accommodated within the present AGS building. Although the dipole has no beneficial optical effects it does serve to

sweep out off momentum particles and prevent them from hitting detectors between MS1 and S4.

The electrostatic separator design is based on that of the KEK K2 beam line separators [2,9] with separated E and B fields (E1,2 and CM1–4 in fig. 2) and electrostatic power supplies that mount directly on the separator vacuum tanks. These features allow about 35% more voltage to be applied to the separator plates than with conventional power supplies and long charging lines.

2.3. Optical properties

The beam line was designed using TRANSPORT [11], DECAY TURTLE [12] and RAYTRACE [13] programs. TRANSPORT was used to determine the first and second order focusing properties of the beam line and DECAY TURTLE was used to determine the acceptance and phase space properties of the beam. RAYTRACE, a ray tracing program correct to all orders in the median plane, was then used to evaluate higher order aberrations in the beam line. Finally, after applying third order corrections to the beam line optics, acceptance and phase space of the beam were determined using RAYTRACE.

Graphs of some first order properties of the beam line are shown in fig. 3. As can be seen, the beam optical design is basically symmetric about the mid-point of the beam line. The first through third order focusing conditions are listed in table 2. In addition to varying the quadrupoles, sextupoles and octupoles, the bend angle of the last dipole, D3, was chosen to make the dispersion $x/\delta \sim 0$ at the final focus (FF).

The quadrupoles (Q2–Q7) used for this beam have diameters (30 cm) comparable to their iron length (41 cm). This leads to significant fringe field effects that cannot properly be treated using conventional TRANSPORT or TURTLE programs. These effects

Table 2

Focusing conditions for 2 GeV beam line. The notation follows the TRANSPORT [11] and RAYTRACE [13] formalism. The factors y/ϕ , $y/\theta^2\phi$ etc., are the transfer coefficients. For example, the vertical image at MS1 (y_{MS1}) is given in terms of the initial phase space coordinate at the production target by: $y_{MS1} = (y/x)x_i + (y/\theta)\theta_i + (y/y)y_i + (y/\phi)\phi_i + (y/\delta)\delta_i + (y/\theta\delta)\theta_i\delta_i + (y/\theta\phi)\theta_i\phi_i +$ other second and higher order terms. x_i etc. represent the initial beam phase space.

Z [m]	Element	First	Second	Third
15.2	MS1	$y/\phi = 0$ $y/y = -1.0$	$y/\phi\delta = 0$ $y/\theta\phi = 0$	$y/\phi\delta^2 = 0$ $y/\theta\phi\delta = 0$ $y/\theta^2\phi = 0$
15.8	Hodo	$x/\theta = 0$ $\theta/\delta = 0$	$\theta/\delta^2 = 0$	
27.9	MS2	$y/\phi = 0$ $y/y = +1.0$	$y/\phi\delta = 0$ $y/\theta\phi = 0$	$y/\theta^2\phi = 0$ $y/\phi\delta^2 = 0$
30.4	DC1	$x/\phi = 0$ $\theta/\delta = 0$	$\theta/\delta^2 = 0$	
31.4	FF	$y/\phi = 0$		

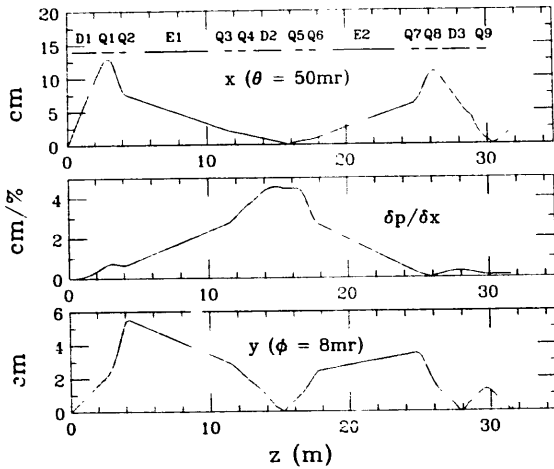


Fig. 3. Some first order TRANSPORT properties of the beam line. The x profile represents the beam half-width for rays with $\delta p/p = 0\%$ and $\delta\theta = 50$ mrad. Similarly the y profile is the half-width for rays with an initial 8 mrad vertical divergence. The center graph shows the variation of the dispersion as a function of distance along the beam line.

lead to third and higher order aberrations of the beam which, if left uncorrected, result in a predicted 30% increase in the rms vertical width of beam at the first mass slit. Fig. 4 shows the effect of the first three octupoles on the most significant third order aberrations affecting the vertical beam width at the first mass slit. These third order aberrations coefficients were calculated using RAYTRACE with a point source input with and $\theta = \pm 35$ mrad and $\phi = \pm 7$ mrad. The usual set [13] of 14 rays was used to determine the

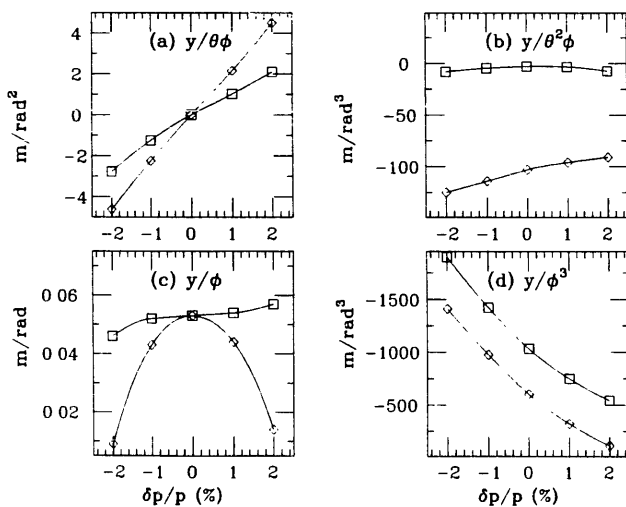


Fig. 4. Important third order aberrations at the first mass slit for the 2 GeV/c beam line as a function of momentum. The diamonds represent the second order beam line solution while the squares show the effect of third order optimization with three octupoles.

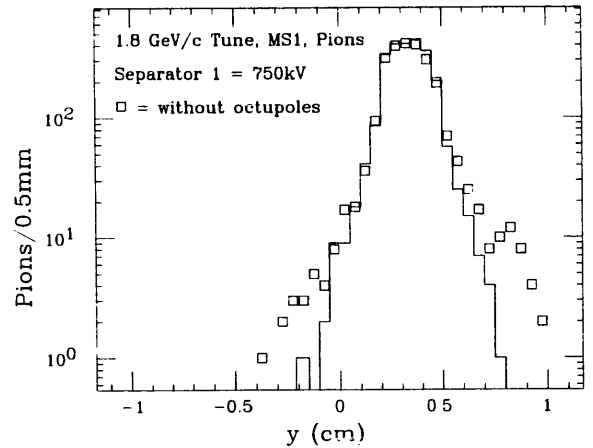


Fig. 5. The calculated pion image at MS1 for a 1.8 GeV/c tune. The image without octupole corrections is indicated by the boxes.

aberrations. The aberration shown in fig. 4a is of the form $y/\theta\phi\delta$ while fig. 4c shows a $y/\phi\delta^2$ variation. The aberration shown in fig. 4d is actually a combination of a fourth order $y/\phi^3\delta$ and aberration and y/ϕ^3 . The y/ϕ^3 part is, in fact, made worse as a result of the third order optimization. The y/ϕ^3 term, as a contribution to the vertical image size, was minimized by a first order change in the vertical focus so that for the maximum vertical angular acceptance, 7 mrad, the condition

$$y/\phi(\Delta\phi) \cong -(y/\phi^3)(\Delta\phi)^3,$$

was satisfied. For $\delta p/p = 0\%$ this condition is satisfied with $y/\phi = +0.05$ m/rad and $y/\phi^3 = -1000$ m/rad³, the values are shown in figs. 4c and 4d, respectively. The net result is a partial cancellation of the third order y/ϕ^3 term with the first order y/ϕ term.

Fig. 5 shows the result of a RAYTRACE Monte Carlo study of the vertical pion image at the first mass slit with and without third order corrections applied. The simulation is for a 1.8 GeV/c momentum beam with the first separator set to transmit kaons through the mass slit. As can be seen, there is a significant difference between the two distributions in the region overlapping $y = 0$. In fact, the predicted number of pions transmitted through a 3 mm MS1 is about a factor of 2 higher for the uncorrected case. The third order corrected RAYTRACE distribution shown in the figure is approximately the same as predicted by the DECAY TURTLE program.

2.4. Collimators

The beam line design incorporates a number of special purpose collimators. These collimators serve not only to stop unwanted particles (mostly pions) that

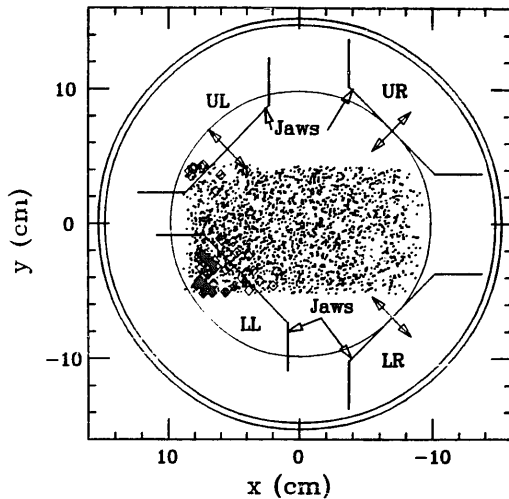


Fig. 6. The beam x, y distribution at the center of the four-jaw collimator. The four-jaws are labeled UL, UR, LL, LR corresponding to upper left, upper right, lower left, and lower right as seen by the beam going into the collimator. The dots and diamonds represent kaons and pions respectively that will pass through a 3 mm first mass slit opening with a 1.8 GeV/c beam line tune and a 750 kV first separator. The solid rectangles are for pions that are transmitted through MS2 to the final focus with a -750 kV second separator and a 4 mm MS2 opening. The LL and UL jaws are shown partially inserted (see text). The jaws can be individually inserted radially inward up to 5 cm.

originate from the kaon production target but also to help eliminate particles from extended sources such as particles that scatter from vacuum pipes, particles from hyperon and meson decay near the target and kaon and pion decays in the beam line. A description of the collimators follows.

2.4.1. Four-jaw collimator

This collimator is located inside a 30 cm diameter vacuum pipe and is centered at the entrance to the first sextupole (S1). A schematic of the collimator jaws as seen by the beam is shown in fig. 6. Each of the jaws is 35 cm long in the beam direction and can be independently positioned. The jaws are made of copper and are driven remotely by stepping motors. Fully inserted, the jaws remove about 60% of the beam acceptance. The beam at this point is approximately parallel and there is a correlation between position (x, y at collimators) and θ, ϕ at the production target. The four-jaw collimator is, therefore, a θ - ϕ collimator and effectively reduces the θ, ϕ phase space.

Fig. 6 shows an x, y plot (at the four-jaw collimator location) of kaons (dots) and pions (diamonds) that originate at the production target and are transmitted through the first mass slit to the downstream detectors. This RAYTRACE Monte Carlo simulation clearly

shows that the four-jaw collimator can be used to eliminate, or at least minimize, the direct pion beam contamination. Fourteen of the 38 pions transmitted through the first mass slit in this simulation will pass through the second mass slit to the final focus (solid rectangles) and are predicted to contribute about 2:1 to the π^-/K^- ratio. The LL jaw is shown in fig. 6 set to eliminate these pions. Also, the UL jaw is shown partially inserted to eliminate some of the pions that would be transmitted to the detectors downstream of MS1.

Extended sources (from slit scattering, decays, etc.), however, cannot be eliminated with this collimator since the θ - ϕ angles projected back to the production target no longer correlate well with position at the four-jaw collimator.

2.4.2. Horizontal slits (HS)

Two horizontal jaws are located inside the vacuum box of the second dipole. Each jaw is remotely movable with its center located about 2 m upstream of the first horizontal focus in the beam line. The collimator can only be used to crudely limit the momentum spread in the beam since position and momentum are not well correlated. These jaws do, however, represent the first well defined horizontal aperture in the beam. The positioning of these slits is predicted to have only a small effect on the beam purity. Each jaw is made of hevimet, a tungsten alloy, and is 40 cm thick in the direction of the beam. This thickness insures that 2 GeV/c muons that enter the collimator will be sufficiently degraded in momentum to be swept away from the experimental detectors at the exit of D2.

2.4.3. Mass slit #1 (MS1)

This slit is located in air inside the second dipole. Each of the two jaws is 5 cm thick vertical by 40 cm horizontal by 90 cm in the beam direction. This slit is located at the first vertical waist. The vertical waist is corrected to second order with $y/\phi\delta = y/\theta\phi = 0$ and to third order with $y/\theta^2\phi \sim 0$, $y/\phi\delta^2 \sim 0$, and $y/\theta\phi\delta$ minimized. (See section 2.3 and fig. 4.) The slit opening is remotely adjustable from about 0.5 to 19 mm. Jaw profiles were made to follow the kaon beam profile and were approximated by three flat surfaces per jaw.

2.4.4. Mass slit #2 (MS2)

This slit is located in the middle of the last dipole vacuum box at the second vertical waist and can be opened from 0.5 to 12 mm. This mass slit has the same dimensions as MS1, and as with MS1, this slit can be remotely positioned and is controlled by stepping motors. Unlike MS1, the MS2 vertical center line can be varied by ± 6 mm, thus allowing the vertical beam position at the experiment's target to be adjusted. Vertical focusing constraints at this position are the

same as MS1 except only $y/\theta^2\phi$ and $y/\theta\delta^2$ need be corrected to third order.

2.4.5. Fixed collimators

Brass and hevimet fixed collimators were provided inside both D2 and D3 to block the gaps between the mass slits and the dipole return yokes (pole tips). Horizontal collimators that follow the beam profile were also included inside both dipoles. Furthermore, a rectangular pipe (11 cm \times 4.3 cm) was inserted into the 20 cm diameter vacuum pipe of the last quadrupole, Q9 and the space between the two pipes filled with 1.2 mm diameter lead shot. The inside dimensions of these collimators were chosen to not intercept the primary beam.

2.5. Electrostatic separators

The separators follow the design of the KEK K2 beam line separators [2]. Electric and magnetic fields are separated to allow higher voltage to be achieved without breakdown due to the Penning effect. Power supplies for the separators are mounted directly onto the separator tanks as with the KEK K2 separators. The proximity of power supplies to separator plates minimizes the stored energy, thus allowing high voltage breakdown inside the separators with little chance of damage to the separator plates. The power supplies were made by the Nichicon Corp. of Japan and were loaned to BNL by KEK. Conventional power supplies available at BNL could not be closely coupled to the separators.

The separator cathodes are made of anodized aluminum and the anodes of stainless steel. The plates are 39 cm wide and are 10 cm apart. Both separators, E1 and E2, are built in two sections, each section containing 2.25 m long plates. The surface flatness and parallelism of the plates is such that the integral of the variations along the length of the plates was less than one part in a thousand across the 20 cm horizontal width of the beam.

The separators normally operate at a pressure of a few $\times 10^{-4}$ Torr of He–Ne (35–65%). The mixture was chosen based on a study at KEK by Yamamoto et al. [14]. The separators must be voltage conditioned in hard vacuum (1×10^{-6} Torr) prior to operation. The conditioning process affects the maximum achievable voltage with gas and the ultimate spark rate. Once the conditioning process is complete, the performance of the separator can be evaluated by plotting the maximum voltage as a function of gas pressure. A plot of the maximum voltage as a function of gas pressure for various levels of hard vacuum conditioning is shown in fig. 7. The minimum level of conditioning required for stable, long-term operation is about 175 kV per plate. Technical difficulties (vacuum leaks and gas pressure

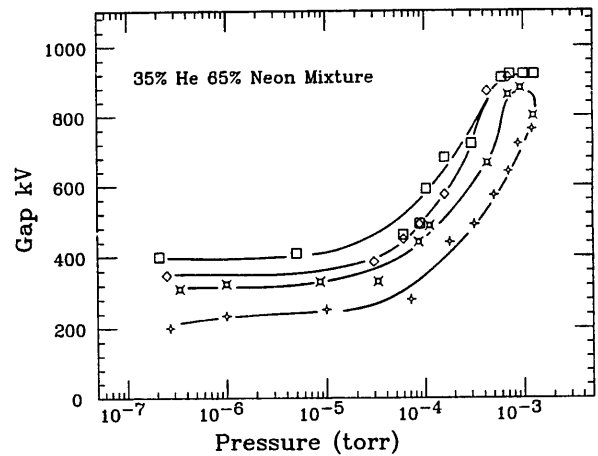


Fig. 7. A graph of separator voltage vs gas pressure for a 35% helium, 65% neon gas mixture. The graph was obtained by fixing the pressure on the separator tank and raising the high voltage until breakdown occurs. The four different curves show the effect of hard vacuum conditioning (10^{-6} Torr) to 200, 300, 350 and 400 kV, respectively.

monitoring problems) during the 1991 commissioning run prevented the separators from running above about 600 kV total. These difficulties have been remedied and both separators have since run at 750 kV per plate for several days with spark rates of less than 10/h.

3. Magnetic field measurements

As can be seen in fig. 2, magnetic elements are closely packed. Close spacing of the magnetic elements is desirable in order to minimize the total beam length and thus minimize kaon losses through decay. Close packing, however, results in the iron of adjacent elements affecting each other's magnetic fields. In order to properly account for these effects field maps of the elements were obtained with adjacent elements in place.

Quadrupole, sextupole and octupole field measurements included magnetic field integrated over length as a function of current. These measurements were made by rotating a long coil about the element's longitudinal axis and extracting the appropriate field component through harmonic analysis. Similar measurements were made for the 8D8 correction dipoles (CM1–4 fig. 2). In addition to the basic field integral measurements, higher order harmonics were determined. Generally, higher order harmonics were small enough to not cause a noticeable change in optical properties of the beam line. Significant higher order aberrations were however found for the 8D8 correction dipoles and quadrupoles that were in close proximity to sextupoles. The 8D8s were found to have a 2.4% sextupole component, relative to the dipole strength, at

the 7.9 cm measuring coil radius. Furthermore, this sextupole component was skewed with respect to the normal beam line sextupole orientation. Iron shims inserted in the dipoles gap corners were found to reduce sextupole component by a factor of 10. A TURTLE simulation predicts that, if left uncorrected, the 8D8 sextupole aberration would cause an 18% increase in the MS1 vertical image width.

It was also found that an unshielded sextupole magnet in proximity to a quadrupole induced an unacceptable octupole component (about 0.5% at a 13.8 cm radius) into the quadrupole. The induced octupole, like the 8D8 sextupole, was skewed with respect to the normal beam line octupole orientation. This magnetic

“crosstalk” is caused by the shortness of the magnets and the physical proximity of their poles. End flux from the quadrupole couples to the poles of the sextupole, breaking the fourfold symmetry and superimposing a weaker twofold symmetry, resulting in the octupole moment. This problem was corrected by adding 1.2 cm thick iron shield plates with a circular hole between the sextupoles and quadrupoles to decouple the fields of the two magnets.

In order to properly evaluate quadrupole and dipole fringe field effects on focusing, the field or field gradient as a function of longitudinal position was measured for selected elements. These measurements were made with adjacent elements installed to properly account

Table 3
Design parameters

Momentum range	up to 2 GeV/c	
Target (length × width × height)	9 × 0.7 × 1.0 cm platinum	
Central production angle	5°	
Horizontal acceptance (FWHM)	+ 55, – 35 mrad	
Vertical acceptance (FWHM)	+ 7, – 6 mrad	
Momentum acceptance (FWHM)	± 3%	
Separators (E1&E2)	750 kV, 4.5 m long (each), 10 cm gap	
Mass slit 1 (TURTLE)		
Vertical magnification	– 1.0	
π–K separation at 1.8 GeV/c	0.34 cm	
Pion image size (rms)	0.096 cm, no multiple scattering	
	0.097 cm, normal multiple scattering ^a	
First horizontal focus (Hodo in fig.2)		
Horizontal magnification	– 9.6	
Dispersion	4.5 cm/%	
Mass slit 2 (TURTLE)		
Vertical magnification	+ 1.0	
π–K separation at 1.8 GeV/c	0.58 cm (MS1 open)	
Pion image size (rms)	0.116 cm (no multiple scattering, MS1 open)	
	0.125 (normal multiple scattering, MS1 = 3 mm) ^b	
Final Focus (TURTLE)		
	Horizontal focus	Horizontal Waist
	at DC1 (table 2)	at 31.4 m
Horizontal image size (rms)	2.1 cm	1.5 cm
Horizontal divergence (rms)	14.2 mrad	7.0 mrad
Vertical image size (rms)	0.1 cm	0.1 cm
Vertical divergence (rms)	4.7 mr	4.7 mr
Momentum spread (rms)	2.0%	2.0%
Solid angle–momentum acceptance (RAYTRACE)	7.90 msr % (no multiple scattering)	
MS1 = 3 mm, MS2 = 4 mm	6.52 (normal multiple scattering) ^b	
	6.17 msr % (normal multiple scattering with four-jaw cut to eliminate direct πs)	
Kaon flux, 1.8 GeV/c K [–] /10 ¹³ protons	2.9 × 10 ⁶ /spill	
Normal multiple scattering ^b		
and four-jaw set to eliminate direct πs		
Direct π [–] /K [–] @ 1.8 GeV/c (RAYTRACE)	2:1 (without four-jaw cut)	
	< 0.5:1 (with four-jaw cut)	

^a 0.0076 cm aluminum vacuum window at entrance to MS1.

^b 0.0076 cm aluminum vacuum window at entrance to MS1, fig. 1 detectors and 0.035 cm Mylar vacuum window at entrance to S4.

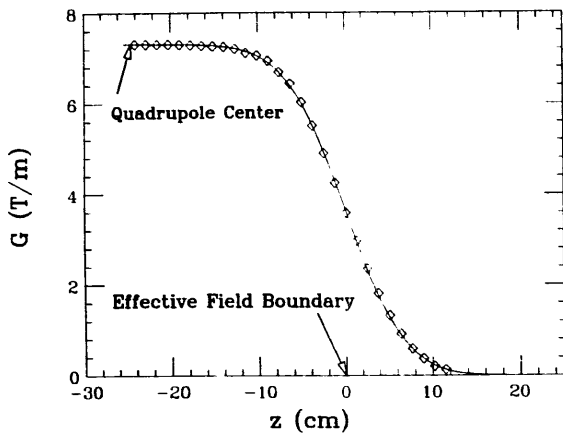


Fig. 8. A graph of the quadrupole field in Q7 as a function of the longitudinal position. $z = 0$ corresponds to the effective field boundary. The measurements were made at a 9.5 cm radius. The diamonds are the measured quadrupole field gradients and the solid line a fit to the data (see text). The parameter of the fit are $c_0 = 0.002$, $c_1 = 8.81$, $c_2 = -0.535$, $c_3 = 11.00$, $c_4 = 10.34$, $c_5 = 2.5$.

for the nearby iron. An example of such a measurement is shown in fig. 8 for one of the quadrupoles. The fit shown in the figure is of the form [13,15]

$$G = G_0 / (1 + e^S),$$

where $S = c_0 + c_1 s + c_2 s^2 + c_3 s^3 + c_4 s^4 + c_5 s^5 + \dots$ and $s = z/d$ (z = longitudinal distance from the effective field boundary and d = diameter of the quadrupole) with $s = 0$ located at the effective field boundary.

This parameterization is appropriate for characterizing quadrupole fields for input to the RAYTRACE program. Parameters of the fit are given in the figure caption. This type of measurement was made only for Q7 and Q8. Other quadrupoles were assumed to have similar fringe field characteristics.

Of the three beam line dipoles, D1-3, only D1 was extensively field mapped. This special purpose dipole was designed in-house. The field inside the dipole is consistent with an ideal sector magnet with no measurable quadrupole or sextupole components. For the uniform field region occupied by the kaon beam, the horizontal field variations are generally less than 0.1% leading to small third and fourth order corrections to the dipole field. RAYTRACE calculations predict a negligible effect on the optical properties of the beam. Both D2 and D3 are generic BNL dipoles and characteristic field maps [10] were assumed to be valid.

4. Predicted performance

The predicted beam performance is shown in table 3. The calculated beam line acceptance is shown under

various conditions, using the RAYTRACE or TURTLE programs as indicated. The beam line will normally be run with detectors between MS1 and S4 (see fig. 2) and with the four-jaw collimator partially closed (see fig. 6) to minimize direct pions at the final focus. It was found that with beam line optics corrected to third order with RAYTRACE, the general properties of the beam agree with TURTLE predictions. TURTLE, however, predicts a direct π/K ratio of less than 0.5:1 at the final focus with the four-jaw collimator fully retracted, whereas RAYTRACE predicts 2:1.

The kaon flux is calculated based on the Sanford-Wang [8] production cross sections for a 24 GeV/c proton beam and a 1.8 GeV/c kaon momentum. The flux calculation assumes the interacting proton fraction is 0.64 (9 cm platinum), the K^- -absorption in the target is 0.85 (assumes proton beam is 1.5 mm from the target edge), the angular acceptance averaged kaon production is 0.05 $K^-/(\text{sr GeV}/c \text{ interacting proton})$ and the K decay factor is 10.2 for the 31.4 m flight path.

The production of antiprotons is expected to be about equal to the K^- production. The antiproton flux will however be reduced due to greater target absorption and multiple scattering losses.

5. The beam line performance

The beam line was commissioned in April 1991 and then used to begin an H particle search experiment [16]. The beam momentum was set at 1.7 GeV/c, lower than the desired 1.8 GeV/c. The lower momentum was chosen to compensate for problems encountered with the separators. The 750 kV design voltage was not achieved until several weeks after the run was over. Furthermore, an early problem with one of the horizontal slits (HS in fig. 2) located inside the D2 vacuum chamber led to the insertion of a vacuum window at the exit of S3. The HS was then left in air for the duration of the 1991 run. The additional multiple scattering of the pions in the S3 window and subsequent 2 m of air to MS1 resulted in a nonnegligible flux of direct pions through MS1 and MS2 to the final focus.

As a consequence of the above problems, the four-jaw and MS1 collimators were closed more than desired. The following conditions prevailed for most of the 1991 commissioning run:

- MS1 = 1.8 mm for kaons, 2.7 mm for antiprotons,
- MS2 = 4 mm for kaons, 5 mm for antiprotons,
- HS = 15% closed,
- Four-jaw LL = closed, UL = 2/3 closed,
- UR = 2/3 closed and LR = open,
- Sep 1 = 590 kV,
- Sep 2 = -600 kV.

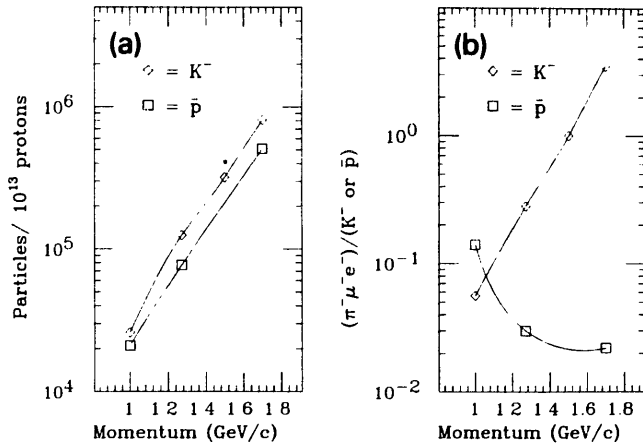


Fig. 9. (a) The measured K^- and \bar{p} flux as a function of momentum. (b) The resulting $(\pi^- \mu^- e^-)/K^-$ or \bar{p} ratios. The flux was measured using the scintillator T2 and a pair of aerogel Cherenkov detectors upstream of T2 to veto pions and muons. The $(\pi^- \mu^- e^-)/(K^- \text{ or } \bar{p})$ ratio was measured using time-of-flight between T1 and T2 (see fig. 1).

With the above conditions the acceptance of the beam line is predicted by RAYTRACE to be reduced to 2.95 msr %. At a 1.7 GeV/c K^- momentum, the predicted (Sanford–Wang) flux is 1.2×10^6 K^- /spill. Furthermore, multiple scattering of pions out of the S3 vacuum window is predicted to result in a 1:1 direct pion contribution to the π^-/K^- ratio at 1.7 GeV/c.

Fig. 9 shows the measured negative kaon and antiproton flux as a function of momentum. As can be seen, even under these less than optimum conditions, beam purity is exceptionally good for a wide range of kaon and antiproton momenta. The $(\pi^- \mu^- e^-)$ to K^- ratio is better than 1:1 for momenta lower than 1.5 GeV/c. For antiprotons the beam purity is generally better than 1:10 $(\pi^- \mu^- e^-)$ to antiproton and in fact is as good as 1:45 at the highest measured momentum, 1.7 GeV/c. Note that the 1.7 GeV/c flux is about 32% lower than that predicted by a RAYTRACE simulator. Furthermore, 1.7 GeV/c $(\pi^- \mu^- e^-)$ is measured to be 3.5:1, whereas the RAYTRACE prediction is 1:1. The remaining 2.5:1 contribution is presumably due to extended sources such as particle decays and slit scattering.

The pure antiproton and low momentum kaon beams are primarily a result of the two-stage separation technique and resulting severe geometric constraints placed on the beam by the two mass slits. Full voltage separators and optimally placed vacuum windows are of critical importance only for higher momentum kaons beams (≥ 1.5 GeV/c), where the π^-/K^- separation at the mass slits is small.

Future runs with this beam line will not have the S3 vacuum window but will have a window at the entrance to MS1, as designed. Furthermore, the separators are

expected to operate at 750 kV rather than 600 kV as in 1991. These improvements are expected to result in better high momentum performance. The changes should allow the four-jaw and MS1 collimators to be opened to desired positions, leading to about a factor of 2 improvement in flux and possibly an improved π^-/K^- ratio.

The beam line tuning time was minimal. The field maps were used together with the RAYTRACE predicted fields to set the magnetic elements. The RAYTRACE predicted field settings for the quadrupoles were from 0.6 to 1.0% higher than TRANSPORT predictions. This is primarily a result of including extended quadrupole fringe fields in the RAYTRACE simulation. After tuning, the quadrupoles remained within 0.5% of the predicted RAYTRACE values. The separator correction magnets CM1–4 and the D2 and D3 dipoles were tuned to adjust the vertical and horizontal alignment of the beam.

The effects of the second and third order correction elements are shown below for a 1.7 GeV/c momentum and the separators set to transmit kaons.

Condition	K^- flux/ 10^{13} protons	$(\pi^- \mu^- e^-)/K^-$
Sextupoles on and Octupoles on	8.1×10^5	3.5:1
Sextupoles off and Octupoles on	7.3×10^5	4.6:1
Sextupoles on and Octupoles off	7.7×10^5	3.8:1

The beneficial effects of the sextupoles is evident; however, the octupoles appear to have only a minor effect. The significance of the octupoles is lessened by the effects of multiple scattering in the S3 vacuum window and because of the tight four-jaw cut (reduced phase space).

6. Concluding remarks

The beam line performance met the design goals with the exception of K^- beam purity at 1.8 GeV/c. However, the exceptional beam purity for both antiprotons and lower momentum kaons verify the effectiveness of the design approach. With full voltage separators and a normal vacuum window configuration, the beam line performance is expected to meet or exceed all design goals.

This beam line is the first of three planned new secondary beam lines at the AGS. The other two include an 800 MeV/c separated particle beam line in support of a stopped K^+ rare decay experiment E787 [17] and an unseparated 6 GeV/c beam line for another rare K^+ decay experiment E865 [18]. These beam lines have been designed to accommodate the

intense proton flux (about a factor of 4 higher than present levels) expected as a result of the ongoing AGS upgrade [7] which includes a new 1.5 GeV booster synchrotron [6].

Acknowledgements

The final design of this beam line is the end result of discussions, began in 1980, among individuals interested in developing a new high purity kaon beam line at the AGS for strange particle physics research. These discussions have included in addition to the authors, D.I. Lowenstein, J.W. Glenn, BNL; H.A. Thiessen, Los Alamos National Laboratory; E. Hungerford, Houston; P.D. Barnes, Carnegie-Mellon University (now at Los Alamos National Laboratory); E. Blackmore, D. Lobb and J. Doornbos, TRIUMF; and many others. The authors are particularly grateful to A. Kusumegi, M. Ieiri, M. Ishii, and M. Takasaki for supplying detailed drawings of the KEK electrostatic separators and for the many helpful discussions about their experience with separators at KEK. We also thank K. Nakai and H. Hirabayashi of KEK for the loan of the electrostatic power supplies currently in use for the separators in this beam line. One of the authors (P. Pile) would like to thank R.T. Ross (Stanford University) who helped with computer simulations of the beam line during his summer internship at BNL in 1989.

Note added in proof

The beam line was again used in 1992 to continue the H-particle search experiment. Although all of the problems associated with the 1991 commissioning run were corrected, a failure in one of the power supplies for the second separator resulted in only 375 kV across its gap (separator 1 ran at the designed 750 kV). Nevertheless, the K^- flux at 1.8 GeV/c was typically of $2.8 \times 10^6 K^-$ per 10^{13} protons with a π^-/K^- ratio of 2.5:1, significant improvements over the commissioning run.

References

- [1] J.D. Fox, BNL EP&S Technical Note nos. 7 (1967) and 20 (1968);
A.S. Carroll, T.F. Kycia, K.K. Li, D.N. Michael, P.M. Mockett, D.C. Rahm and R. Rubenstein, BNL EP&S Technical Report no. 54 (1972).
- [2] A. Yamamoto, H. Ikeda, S. Kurokawa, M. Takasaki, M. Taino, Y. Suzuki, I. Ishii, A. Kusumegi and H. Hirabayashi, Nucl. Instr. and Meth. 203 (1982) 35.
- [3] S. Kurokawa, H. Hirabayashi and E. Kikutani, Nucl. Instr. and Meth. 212 (1983) 91.
- [4] M. Takasaki et al., Nucl. Instr. and Meth. A242 (1986) 201.
- [5] A.B. Dover and A. Gal, Ann. Phys. (NY) 1416 (1983) 309.
- [6] W.T. Weng, Proc. 14th Int. Conf. on High Energy Accelerators, Tsukuba, Japan, 1989, ed. D. Keefe, Part. Accel. 27, Part II (1990) 13.
- [7] Th. Sluyters, *ibid.*, p. 1.
- [8] J.R. Sanford and C.L. Wang, BNL-AGS Internal Reports 11279 and 11479 (1967).
- [9] A. Yamamoto, A. Maki and A. Kusumegi, Nucl. Instr. and Meth. 148 (1978) 203.
- [10] G.T. Danby, BNL-AGS Intl. Report GTD-2.
- [11] K.L. Brown, F. Rothacker, D.C. Carey and Ch. Iselin, CERN 80-04 (1980).
- [12] K.L. Brown and Ch. Iselin, CERN 74-2 (1974).
- [13] S.B. Kowalski and H.A. Enge, Nucl. Instr. and Meth. A258 (1987) 407; and Technical Report 156, Laboratory for Nuclear Science, MIT.
- [14] A. Yamamoto, A. Maki, Y. Maniwa and A. Kusumegi, Jpn. J. Appl. Phys. 16 (1977) 343.
- [15] H.A. Enge, in: *Focusing of Charged Particles*, ed. A. Septier vol. II (Academic Press, New York, 1967) p. 203.
- [16] AGS Exp. 813 and 836, CMU, BNL, Freiburg, Kyoto, Kyoto-Sangyo, Birmingham, New Mexico, Los Alamos National Laboratory, Manitoba, TRIUMF, Vassar, Indiana collaboration, P.D. Barnes and G. Franklin, spokesmen.
- [17] AGS Exp. 787, BNL, Princeton, TRIUMF collaboration, D. Bryman, L. Littenberg and S. Smith, spokesmen.
- [18] AGS Exp. 865, Yale, BNL, INR, Moscow, JINR-Dubna, New Mexico, PSI, Basel, Pittsburgh, Tbilisi State, Zurich collaboration, M. Zeller, spokesman.